A comparison of two numerical approaches for theoretical investigations of thermal tweezers of adatoms on crystalline substrates.

Mark B. Flegg, Daniel R. Mason, Dmitri K. Gramotnev and Galina Gramotnev

Applied Optics and Nanotechnology Program, School of Physical and Chemical Sciences, Queensland University of Technology, GPO Box 2434, Brisbane, QLD 4001, Australia

Abstract

We compare the computational efficiency, accuracy and relative agreement of two numerical approaches to the theoretical investigation of a new technique recently proposed for fabrication of nanostructures on surfaces – thermal tweezers. In this technique, adsorbed particles are thermophoretically redistributed by strong spatial gradients of the surface temperature induced by interfering laser pulses. In principle, the resulting structures are limited only by the type of pattern that can be reproduced holographically which is quite arbitrary. At the same time, subwavelength resolution of structures has been previously predicted. We consider diffusion on a crystalline substrate modelled as a square lattice, sinusoidal, uncoupled periodic potential, and linear frictional dissipation of the particle motion. The temperature on the substrate is strongly modulated sinusoidally along one direction. The first numerical approach is the Monte Carlo (MC) simulations employing the Ermak algorithm as a direct solution of a Langevin equation (LE). The second method is the local solution of the Klein-Kramer equation (KKE) by the matrix continued fraction method (MCFM) to determine local values of the diffusion coefficient. The spatially dependant diffusion coefficient is substituted into a one-dimensional Smoluchowski equation (SE) that is

solved numerically using the finite volume method (FVM) to determine the temporal evolution of the spatial probability density of particles $\phi(x, t)$. Main attention is given to the relative agreement of either approach as the frictional dissipation coefficient γ is varied over several orders of magnitude. We discuss the parameter range over which each method is most suitably applied. In addition, we provide brief physical explanation for several interesting observations relating to optimal values of γ where particles are most efficiently redistributed.

Key Words: Surface diffusion, Thermophoresis, Finite volume method, Langevin equation, Smoluchowski equation, Surface nanostructures, Nanofabrication.

1. Introduction.

Recently, a new approach, called thermal tweezers, has been investigated theoretically for achieving nanomanipulation and significant spatial redistribution of nanoparticles and adatoms on surfaces [1, 2]. This approach is based on surface thermophoresis in the presence of strong temperature gradients produced holographically by means of near-surface absorption of electromagnetic energy in two or more interfering laser pulses. In this case, due to their Brownian motion, the particles or adatoms on the surface experience anisotropic diffusion that is predominantly directed from hot regions to cold regions [1, 2].

It has been demonstrated that one of the major important features of thermal tweezers (thermophoresis on surfaces) [1, 2] is that they could be at least an order of magnitude more efficient in terms of achieving strong particle re-distribution than the conventional thermophoresis in a bulk medium (e.g., liquid) [3, 4]. The typical maximum-to-minimum concentration ratio (in the cold and hot regions) achievable by means of thermal tweezers have been shown to reach up to ~ 100 times at temperature modulations of a few hundreds of degrees on the scale of a couple of hundreds of nanometers [1]. This is because particles or adatoms on a surface diffuse in a periodic (for a crystalline substrate) or random (for an

amorphous substrate) additional potential produced due to the interaction of these particles or adatoms with the surface [1, 2]. The resultant additional potential wells on the surface cause further suppression of particle diffusion in the cold regions, leading to a significantly enhanced concentration modulation for particles or adatoms on the surface [1, 2].

The other important result that has been demonstrated in papers [1, 2] is that thermal tweezers can be used to obtain elements of surface patterning with nano-scale dimensions. For example, using a special superresolution technique [1, 2] the dimensions of the obtained elements on the surface could be in the range of 10 – 100 nm, when using the interfering laser beams in the optical range of frequencies.

Any complex surface pattern with nano-scale elements, which can be achieved using holographic methods, could be reproduced or recorded on a surface by means of surface tweezers. Therefore, potential applications of thermal tweezers include tailoring and precise engineering of optical and electronic properties of surfaces and interfaces, possibility of manipulation and trapping of small nanoparticles and even separate adatoms on surfaces and interfaces with nano-scale resolution, new methods of parallel nanofabrication on surfaces, re-writable memory elements, image recording techniques, etc.

The theoretical analysis of thermal tweezers [1, 2] has so far been based on Monte Carlo (MC) simulations and numerical solution of the Langevin equation by the Ermak algorithm [5]. The periodic surface temperature and periodic potential describing the interaction with the crystalline substrate are included in the Langevin equation. In this approach, the trajectories of individual particles are determined independently. By simulating a large number of individual particle and their trajectories, the probability distribution at any moment of time is determined [1, 2]. The direct simulation of individual particle trajectories enables easy visualization and understanding of particle diffusion on the surface [6]. For example, in a periodic potential of the crystal lattice the motion of individual particles is a combination of

both nearest neighbor hopping and long jumps [7-9]. In nearest neighbor hopping, particles move across the crystal lattice by jumping from one potential well into one of the directly neighboring potential wells. Long jumps occur when the particle hops from one potential well and moves over several or many lattice periods before it becomes trapped in a different potential well [8, 9]. The high-friction regime is dominated by nearest neighbor hopping while the low-friction regime is characterized by a larger proportion of long jumps (i.e., Levy flights resulting in the anomalous surface diffusion[7]).

It is expected that jump length should strongly affect the strength of redistribution of particles into the cold regions in the thermal tweezers technique. It has been predicted that there are optimal values of friction for any given period of the temperature modulation on the surface, which provide the maximal possible modulation of particle concentration as a result of application of thermal tweezers [10]. This is one of the demonstrations of the importance and usefulness of the MC simulation approach, which automatically takes into account any type of short and long jumps. Another significant advantage of the MC simulation approach [1, 2] is that this method allows visualization of particle diffusion similar to how it occurs in a real experiment. This means that non-steady-state particle distributions on a surface can be immediately and directly investigated by means of this method at any evolutionary times[1] and for any number of laser pulse treatments [2].

However, the main disadvantage of the MC approach based on the numerical solution of the Langevin equation is related to its numerical inefficiency. It is based on numerical solution of the Langevin equation for a very large number of particles (up to 50,000 – see Refs 1 and 2). If in addition the time for achieving significant particle re-distribution is much larger than the typical period of particle oscillations in a potential well associated with the interaction between the particle and a node of the crystal lattice of the substrate, then a very large number of time steps (so that to properly resolve the particle motion in the potential

well) should be used. This requires extensive computational resources and time. Statistical analysis of the obtained particle distributions could be used to reduce the required number of simulation particles [1, 2], and thus reduce the required computational resources. However, this could only be efficient for not very large evolutionary times. If the typical evolutionary times reach several thousands of nanoseconds, the MC approach is difficult to use, especially if the detailed analysis of impacts of several different parameters (such as, for example, temperature modulation, depth of the potential wells, different friction coefficients, etc.) is required. Furthermore, the MC approach cannot be used to directly analyze the steady-state particle distributions. Statistical methods can be used to extrapolate the obtained results to the steady-state particle distributions[1, 2], but these may lead to noticeable statistical errors, especially when the temporal dependencies of particle concentrations at the minimum and maximum of surface temperature are not simple exponentials or sigmoids (e.g., in the presence of superresolution [1, 2]).

Therefore, the aim of this paper is to introduce and develop a new approach for the analysis of thermal tweezers, based on the direct determination and investigation of probability distributions for diffusing particles or adatoms on a surface in the presence of strong temperature gradients. This will be done by means of numerical finite-volume solution [11] of the Smoluchowski diffusion equation. The local values of the diffusion constant will be determined by solution of the Fokker-Planck equation for the considered crystalline potential of the substrate and local temperature. In particular, this approach will be directly applicable for the analysis of steady-state particle distributions on the surface during the application of thermal tweezers. Detailed comparison of this approach with the previously obtained results from the MC simulations of the Langevin equation [1, 2] will be conducted, demonstrating high computational efficiency and accuracy of the new method in the high-friction regime. However, in the low-friction regime the approach based on the Smoluchowski diffusion

equation will be shown to provide excessively large modulations of particle concentration. This will be explained by the presence of long jumps (Levy flights) in the low-friction regime, which makes the diffusion approximation inapplicable. Applicability conditions for both the approaches will thus be discussed and analyzed.

2. Numerical Methods of Analysis

As was previously done in Refs. 1 and 2, the theoretical analysis of thermal tweezers is conducted on a crystalline surface with a square lattice of period a. Therefore, the periodic potential $V(x,y)$ of interaction between the particle and the crystalline surface is given by [1, 2]:

$$V(x,y) = \frac{V_0}{2}\left[\cos\left(\frac{2\pi x}{a}\right) + \cos\left(\frac{2\pi y}{a}\right)\right], \tag{1}$$

where x and y are the coordinates on the surface, and V_0 is the amplitude of the periodic potential characterizing depth of the potential wells for the particle on the surface ($2V_0$ is the difference between a maximum and a minimum of the periodic potential function $V(x,y)$). The temperature on the surface $T(x)$ is modulated sinusoidally along only the x direction and is given by

$$T(x) = T_0 + \Delta T \cos^2\left(\frac{\pi x}{\lambda}\right), \tag{2}$$

where λ is the period of the temperature modulation which is considered to be much greater than the lattice period $\lambda >> a$.

2.1. Monte Carlo (MC) Simulations

In the Monte Carlo simulation approach [1, 2], the position vector $\mathbf{r} = (x, y)$ for the particles diffusing on the substrate obey the Langevin equation:

$$m\frac{d^2\mathbf{r}}{dt^2} = -m\gamma\frac{d\mathbf{r}}{dt} - \nabla V(\mathbf{r}) + \xi_{\mathbf{r}}(t) \tag{3}$$

where m is the mass of the particles, γ is the frictional dissipation coefficient (units s^{-1}), $V(\mathbf{r})$ is the periodic potential of interaction between the particle and the crystalline surfaced – see Eq. (1), and $\xi_{\mathbf{r}}(t)$ is a stochastic force that describes the Brownian forces due to coupling with a thermal bath (i.e., with the crystalline surface at the local temperature $T(x)$ – Eq. (2)) [12]. The stochastic force obeys the standard fluctuation-dissipation relation [12],

$$\left\langle \xi_i(t)\xi_j(t')\right\rangle = \frac{2\gamma k_B T(x)}{m}\delta_{ij}\delta(t-t') \tag{4}$$

where k_B is the Boltzmann constant, $T(x)$ is given by Eq. (2), the indices i and j run through the values 1 and 2 corresponding to the x-coordinate (index 1) and y-coordinate (index 2) on the surface, and the delta functions indicate zero correlations for the Brownian forces in time and direction (white noise). Eq. (3) is solved numerically by the Ermak algorithm [5] to determine the particle trajectories. The Ermak algorithm is a finite-difference time-domain algorithm, where the position $\mathbf{r}$ and velocity $\mathbf{v}$ of a particle at the time $t+dt$ are determined from its position and velocity at the previous moment of time t according to the expansions [5]:

$$\mathbf{r}(t+dt) = \mathbf{r}(t) + c_1\mathbf{v}(\mathbf{t})dt + c_2\frac{\mathbf{F}(t)}{m}dt^2 + c_3\frac{\dot{\mathbf{F}}(t)}{m}dt^3 + \delta\mathbf{r}^G, \tag{5a}$$

$$\mathbf{v}(t+dt) = c_0\mathbf{v}(t) + c_1\frac{\mathbf{F}(t)}{m}dt + c_2\frac{\dot{\mathbf{F}}(t)}{m}dt^2 + \delta\mathbf{v}^G. \tag{5b}$$

Here, $\mathbf{F} = \left(-\partial V(\mathbf{r})/\partial x, -\partial V(\mathbf{r})/\partial y\right)$, $\dot{\mathbf{F}}$ denotes differentiation of $\mathbf{F}$ with respect to time, and the coefficients c_i are determined by the equations:

$$c_0 = \exp(-\gamma dt), \tag{6a}$$

$$c_1 = (\gamma dt)^{-1}(1-c_0), \tag{6b}$$

$$c_2 = (\gamma dt)^{-1}(1-c_1), \tag{6c}$$

$$c_3 = (\gamma dt)^{-1}(0.5 - c_2). \tag{6d}$$

The position increment $\delta\mathbf{r}^G$ and velocity increment $\delta\mathbf{v}^G$ are due to the stochastic force and determined by sampling from the bivariate Gaussian distribution[5]:

$$\rho(\delta r_{i\alpha}^{\mathrm{G}}, \delta v_{i\alpha}^{\mathrm{G}}) = \frac{1}{2\pi\sigma_r\sigma_v(1-c_{rv}^2)^{1/2}}$$

$$\times \exp\left\{-\frac{1}{2(1-c_{rv}^2)} \times \left[\left(\frac{\delta r_{i\alpha}^{\mathrm{G}}}{\sigma_r}\right)^2 + \left(\frac{\delta v_{i\alpha}^{\mathrm{G}}}{\sigma_v}\right)^2 - 2c_{rv}\left(\frac{\delta r_{i\alpha}^{\mathrm{G}}}{\sigma_r}\right)\left(\frac{\delta v_{i\alpha}^{\mathrm{G}}}{\sigma_v}\right)\right]\right\}, \tag{7}$$

where

$$\sigma_v^2 = \left\langle \left(\delta v_{i\alpha}^G\right)\right\rangle = \frac{kT}{m}(1 - \exp[-2\gamma dt]), \tag{8a}$$

$$\sigma_r^2 = \left\langle \left(\delta r_{i\alpha}^G\right)\right\rangle = dt^2\,\frac{kT}{m}\frac{1}{\gamma dt} \times \left[2 - \frac{1}{\gamma dt}(3 - 4\exp[-\gamma dt] + \exp[-2\gamma dt])\right], \tag{8b}$$

$$c_{rv} = dt\,\frac{kT}{m}\frac{1}{\sigma_r\sigma_v}\frac{1}{\gamma dt}(1 - \exp[-\gamma dt])^2. \tag{8c}$$

The spatial domain of the simulations is given by the inequalities $0 < x \leq \lambda$ and $0 < y \leq \lambda$. This spans one full period of the temperature modulation. Periodic boundary conditions are imposed at the boundaries of the computational domain, which means that particles leaving the domain emerge at the opposite side of it with the same velocity. The simulation of a sufficiently large number of particle trajectories (~ 50,000 when λ ~ 100 nm) in the computational domain with the subsequent statistical smoothing (using the moving average technique) enables the determination of spatial probability density of particles at any moment of time as a function of the *x*-coordinate [1, 2].

2.2 Smoluchowski diffusion equation

This section outlines a new approach for the analysis of thermal tweezers, in which the probability density is determined directly without the statistical analysis of particle positions on the surface at different moments of time (as was done in the MC simulation approach). Because the *x*- and *y*-components of the force derived from the interaction potential (1) do not depend only on the *y*- and *x*-coordinates, respectively, motion of the particles can be considered independently along the *x*- and *y*-directions on the surface. At the same time, the temperature is modulated only in the *x*-direction. Therefore, diffusion in the *y*-direction is uniform which implies that the probability density along this component will also be uniform. In this case the problem can be reduced to one-dimensional diffusion along the *x*-axis, described by the one dimensional Smoluchowski diffusion equation (SE) for the probability density function $\phi(x,t)$ [13]:

$$\frac{\partial \phi}{\partial t} = \frac{\partial^2}{\partial x^2}\left[D(x)\phi(x,t)\right] \tag{9}$$

where $\phi(x,t)dxdt$ is the probability to find a particle between the positions x and $x + dx$ at moment of time between t and $t + dt$, and $D(x)$ is the spatially dependant diffusion coefficient that is to be determined. Eq. (9) is solved over one full period of the temperature modulation, that is, on the spatial domain $0 < x \leq \lambda$. The spatial dependence of D is easily understood, as it is directly related to the rate at which particles hop between neighbouring potential wells on the surface (see Eq. (1)), which is a thermally activated process.

Eq. (9) is a conservation equation. Therefore, it can be effectively solved by the numerical finite-volume solution method (FVM) [11]. In this approach, the computational window is divided into grid cells which are referred to as control volumes (Fig. 1). Eq. (9) is integrated across the control volume from x_w to x_e which gives

$$\frac{\partial \phi(x_P,t)}{\partial t}\Delta x_P = D(x_e)\frac{\partial \phi(x_e,t)}{\partial x_e} + \frac{\partial D(x_e)}{\partial x_e}\phi(x_e,t) -$$

$$- D(x_w)\frac{\partial \phi(x_w,t)}{\partial x_w} - \frac{\partial D(x_w)}{\partial x_w}\phi(x_w,t), \tag{10}$$

where the integral of the time derivative in Eq. (9) is approximated by $\frac{\partial \phi(x_P,t)}{\partial t}\Delta x_P$, x_P is the x-coordinate of the point P in Fig. 2, $\Delta x_P = x_e - x_w$, and w and e denotes the west and east control volume faces, respectively. Integrating Eq. (10) once again over a time step δt from $t = t_n$ to $t = t_{n+1}$ gives,

$$\begin{aligned}\phi_P^{n+1} - \phi_P^n = \frac{\delta t}{\Delta x_P}\Bigg[\theta\Bigg(& D(x_e)\frac{\partial \phi(x_e,t_{n+1})}{\partial x_e} + \frac{dD(x_e)}{dx_e}\phi(x_e,t_{n+1}) - \\ & - D(x_w)\frac{\partial \phi(x_w,t_{n+1})}{\partial x_w} - \frac{dD(x_w)}{dx_w}\phi(x_w,t_{n+1})\Bigg) + \\ & + (1-\theta)\Bigg(D(x_e)\frac{\partial \phi(x_e,t_n)}{\partial x_e} + \frac{dD(x_e)}{dx_e}\phi(x_e,t_n) - \\ & - D(x_w)\frac{\partial \phi(x_w,t_n)}{\partial x_w} - \frac{dD(x_w)}{dx_w}\phi(x_w,t_n)\Bigg)\Bigg],\end{aligned} \tag{11}$$

where $\phi_P^n \equiv \phi(x_P,t_n)$ (the other similar notations are introduced in the same way), and θ is the temporal weighting coefficient: $\theta = 1$ defines the fully implicit method [11], and $\theta = 0.5$ defines the Crank-Nicolson method [11]. In this paper, we choose to use the Crank-Nicolson method because it is inherently more accurate and has better convergence [11]. Standard first order approximations are used to discretize the derivatives of ϕ at the control volume faces. For example,

$$\frac{\partial \phi(x_e,t_{n+1})}{\partial x_e} \approx \frac{\phi_E^{n+1} - \phi_P^{n+1}}{x_E - x_P} \tag{12}$$

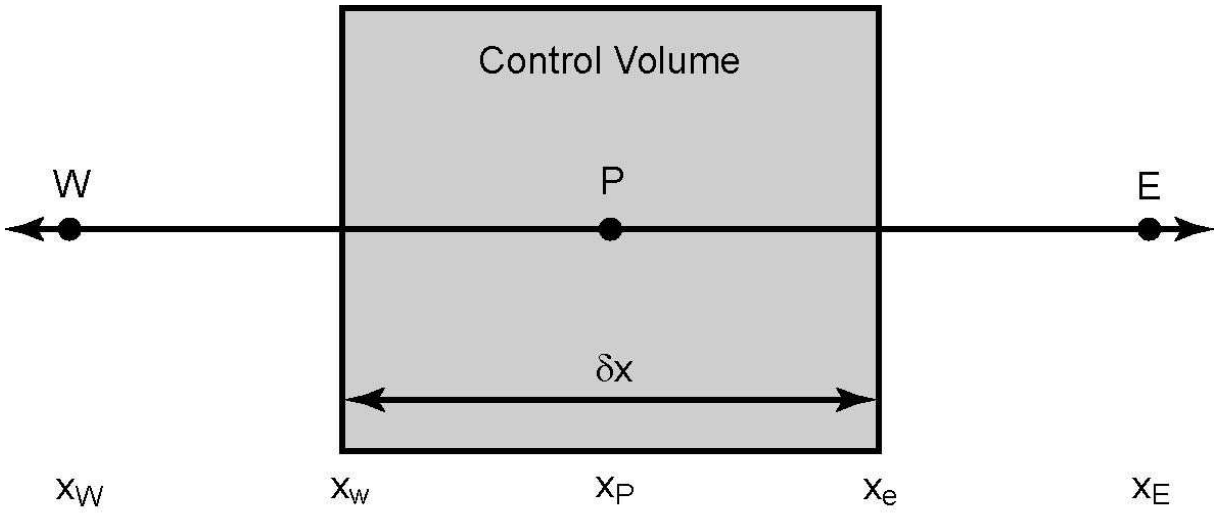

Figure 1: An arbitrary control volume within the computational domain.

This gives a set of linear equations in the unknowns $(\ldots, \phi_W, \phi_P, \phi_E, \ldots)$ at each of the internal node points. Employing periodic boundary conditions, we equate the east face of the right most control volume (at $x = \lambda$) with the west face of the left most control volume (at $x = 0$). Due to the symmetry of the domain the east point, *E*, for the right hand boundary control volume will be the first control point in from the left hand side of the domain. Similarly, the west point, *W*, for the left hand boundary control volume is the last control volume within the domain. The linear system of equations in ϕ at each control volume boundary are solved at time step t_{n+1} from the ϕ determined at the previous moment of time t_n. A more detailed discussion of the FVM can be found in Ref. 11.

2.3 Approximation of the diffusion constant *D(x)*

In a potential well structure such as that described by Eq. (1), there are two main factors that determine the diffusion constant of particle motion; the jump rate and the jump length. The jump rate is the rate which a particle is thermally activated to escape a potential well.

Obviously the jump rate is related to the potential well depth, and the local temperature; increasing the temperature will decrease the typical time required for a particle to gain sufficient thermal energy to escape [7]. On escape from a well, a particle will undergo ballistic motion dissipated by a non-adiabatic coupling with the surface described as a linear frictional dissipation of the motion. When sufficient kinetic energy has been dissipated, the particle no longer possesses sufficient energy to traverse a potential barrier between neighboring wells. Therefore, the particle will once again become trapped in a potential well. The average distance a particle travels between successive escape and trapping events is called the jump length. There is a simple relationship that links these quantities together for periodic potential structures [7].

$$D = a_n r_j \left\langle l^2 \right\rangle, \tag{13}$$

where D is the effective diffusion constant, r_j is the total jump rate, $\left\langle l^2 \right\rangle$ is the mean-square jump length and a_n is contextual and depends on the number of equivalent escape routes for the Brownian particle from a particular well [7]; a_n = ½ for a one dimensional periodic potential well structure, and a_n = ¼ for a two-dimensional potential with four equivalent escape routes which is the case for the considered potential (1). There is numerous literature on approximate methods for determining r_j and $\left\langle l^2 \right\rangle$ [14-16]. The simplest approximation is that of the high-friction limit, in which r_j is determined by Kramer's equation and the jump length is set equal to the distance between neighboring potential wells $\left\langle l^2 \right\rangle = a^2$. The latter is justified since in the high friction regime the particle motion is dominated by nearest neighbor hopping.

The diffusion constant can be rigorously determined by the numerical solution of the KKE by the Matrix Continued-Fraction Method (MCFM). We give brief details of this method here but a full explanation can be found in reference [13]. Specifically, an effective mobility of the particles is determined across each lattice spacing by the local solution of the

KKE at nodal points on the spatial domain (computational domain) across which the surface temperature can be considered constant. The general KKE for the phase space probability density $W(x, v, t)$ corresponding to the Langevin equation (3) is [13]

$$\frac{\partial W}{\partial t} = \left[-\frac{\partial}{\partial x} v + \frac{\partial}{\partial v}\left(\gamma v + \frac{V'(x)}{m} \right) + \gamma \frac{kT}{m} \frac{\partial^2}{\partial v^2} \right] W , \tag{14}$$

where $W(x, v, t)dxdvdt$ is the probability to find a particle between positions x and $x + dx$ and velocity between v and $v + dv$ at moment of time between t and $t + dt$. The function $V'(x)$ is simply the x component of the force due to the particle substrate interaction; that is, the derivative of the potential in Eq. (1) with respect to x. The temperature T in Eq. (14) is taken to be spatially invariant since we solve Eq. (14) only over a small region across which the temperature is considered constant. The following non-dimensional quantities are introduced, denoted by subscript n;

$$x_n = x\frac{2\pi}{a}; \qquad t_n = t\frac{2\pi}{a}\sqrt{\frac{kT}{m}}; \qquad v_n = v\sqrt{\frac{m}{kT}}; \quad \gamma_n = \gamma\frac{a}{2\pi}\sqrt{\frac{m}{kT}};$$

$$V_n'(x_n) = V'(x)\frac{m}{kT}\frac{a}{2\pi} \tag{15}$$

The KKE in Eq. (14) is rewritten as

$$\frac{\partial W(x_n, v_n, t_n)}{\partial t_n} = \left[-\frac{\partial}{\partial x_n} v_n + \frac{\partial}{\partial v_n}\left(\gamma_n v_n + V_n'(x_n) + \gamma_n \frac{\partial}{\partial v_n} \right) \right] W(x_n, v_n, t_n), \tag{16}$$

where $V_n(x_n) = d\cos(x_n)$, and $d = \frac{V_0}{kT}$.

Since we are only interested to determine an effective mobility, we may consider the steady state KKE with the solution $\overline{W}(x_n, v_n)$,

$$0 = \left[-\frac{\partial}{\partial x_n} v_n + \frac{\partial}{\partial v_n}\left(\gamma_n v_n + V_n'(x_n) + \gamma_n \frac{\partial}{\partial v_n} \right) \right] \overline{W}(x_n, v_n) \tag{17}$$

The solution to Eq. (17) can be written as the sum [13],

$$\overline{W}(x_n, v_n) = \psi_0(v_n)\sum_{i=1}^{\infty} c_i(x_n)\psi_i(v_n) \tag{18}$$

where $\psi_i(v_n) = \mathrm{H}_i\left(v_n/\sqrt{2}\right)\exp\left(-v_n^2/4\right)/\sqrt{i!2^i\sqrt{2\pi}}$, and H_i is the *i*th Hermite polynomial. Substitution of Eq. (18) into (17) gives a linear system of partial differential equations for the functions $c_i(x_n)$ in the expansion (18).

$$0 = \begin{bmatrix} 0 & \sqrt{1}\mathbf{D}' & 0 & 0 & 0 \\ \sqrt{1}\hat{\mathbf{D}}' & 1\gamma & \sqrt{2}\mathbf{D}' & 0 & 0 \\ 0 & \sqrt{2}\hat{\mathbf{D}}' & 2\gamma & \sqrt{3}\mathbf{D}' & 0 \\ 0 & 0 & \sqrt{3}\hat{\mathbf{D}}' & 3\gamma & \sqrt{4}\mathbf{D}' \\ \cdots & \cdots & \cdots & \cdots & \ddots \end{bmatrix} \begin{bmatrix} c_0 \\ c_1 \\ c_2 \\ c_3 \\ \vdots \end{bmatrix} \tag{19}$$

where $\mathbf{D}'$ and $\hat{\mathbf{D}}'$ are the operators $\mathbf{D}' = \partial/\partial x$ and $\hat{\mathbf{D}}' = \partial/\partial x + V_n'$. The first equation in this system (19) implies $c_1 = c$ = const. We note that the effective diffusion constant at the node *P* in the FVM can be written [13],

$$D(x_p) = \gamma_n \mu_n D_{flat}(x_p), \tag{20}$$

where $D_{flat}(x_p) = kT(x_P)/(m\gamma)$ is the well known diffusion constant in a uniform (flat) potential at the point x_P, and γ_n is simply the non-dimensionalized friction coefficient (the same used in the MC approach but dimensionless), and μ_n is the called the effective mobility. Note the *x* dependence of D_{flat} is due only to the spatial dependence of the surface temperature according to Eq. (2). To define the effective mobility, a small non-dimensional force δF_n is introduced.

$$\mu_n = \frac{\langle v_n \rangle}{\delta F_n}, \tag{21}$$

where $\langle v_n \rangle$ is the thermal-averaged velocity of particles in a potential due to the small unbalanced force δF_n. It is evident from the definition of μ_n that it is the inverse of an effective friction in response to the small force δF_n. The small force is included in the KKE as a small perturbation to $V_n'(x_n)$.

$$V_n'(x_n) = \lim_{\delta F \to 0}\left(V'(x)\frac{m}{kT}\frac{a}{2\pi} - \delta F_n \right) \tag{22}$$

From the definition of $\overline{W}(x_n, v_n)$, and the properties of functions $\psi_i(v_n)$ and $c_i(x_n)$ one can show,

$$\langle v_n \rangle = \int_0^{2\pi}\int_{-\infty}^{\infty} v_n \overline{W}(x_n, v_n) dv_n dx_n = \int_0^{2\pi}\int_{-\infty}^{\infty} v_n \psi_0(v_n) \sum_{i=1}^{\infty} c_i(x_n)\psi_i(v_n) dv_n dx_n = 2\pi c \tag{23}$$

Therefore we can write $\gamma_n \mu_n = \dfrac{2\pi c \gamma_n}{\delta F_n}$ and the task is to determine the constant *c* by the MCFM. According to the MCFM, the constant *c* is determined numerically by evaluation of

$$c = \frac{1}{2\pi H_{00}}, \tag{24}$$

where $\mathbf{H} = -\gamma_n \hat{\mathbf{D}}^{-1}\mathbf{M}_1$. The matrix $\mathbf{M}_1$ is found from the recurrence relation $\mathbf{M}_i = \mathbf{I} - \dfrac{1}{i\gamma_n}\mathbf{D}\mathbf{M}_{i+1}^{-1}\hat{\mathbf{D}}$, starting at $\mathbf{M}_{N0} = \mathbf{I}$, where $N0 \sim 20/\gamma_n$ and $\mathbf{I}$ is the identity matrix with the elements $\mathrm{I}_{qp} = \delta_{qp}$, δ_{qp} is the Kronecker delta. The elements of $\hat{\mathbf{D}}$ and $\mathbf{D}$ are given by $\hat{D}_{pq} = (iq - \delta F)\delta_{pq} - i(\delta_{p,q+1} - \delta_{p,q-1})d/2$, $D_{pq} = iq\delta_{pq}$, where $i = \sqrt{-1}$ (the reader is directed to reference [13] for a derivation of Eq. (24)). The indices *p* and *q* of the matrices $\hat{\mathbf{D}}$, $\mathbf{D}$ and $\mathbf{H}$ range from negative infinity to infinity. We find it sufficient to truncate this range -12 $\leq p \leq$ 12 and -12 $\leq q \leq$12, such that $\hat{\mathbf{D}}$, $\mathbf{D}$ and $\mathbf{H}$ are 25 × 25 element matricies. For

numerical purposes we typically found that $\delta F_n = 10^{-6}$ was small enough for the full range of parameters we investigated.

In summary, the basic steps to determine the probability density $\phi(x,t)$ are as follows. The constant *c* is determined numerically from Eq. (24), and is substituted into $\gamma_n \mu_n = \frac{2\pi c \gamma_n}{\delta F_n}$ to determine the mobility μ_n. The mobility μ_n is substituted into Eq. (20) to determine the diffusion constant $D(x_P)$ at nodal points *P*. The diffusion constant is inserted into the Smoluchowski equation (9) which is solved numerically by the FVM for the probability density $\phi(x,t)$ at each time step by the FVM equation (11).

3. Results and Comparison

Here we present results comparing the two methods. Throughout our discussion we will concentrate mainly on the probability density $\phi(x, t)$ at the position of maximum temperature (at $x = 0, \lambda$) and minimum temperature (at $x = \lambda/2$); we denote these as $\phi_h(t)$ and $\phi_c(t)$. The steady state values of ϕ_h and ϕ_c (i.e. $\phi_{h,c}$ $(t \rightarrow \infty)$) are denoted as Φ_h and Φ_c. Our main focus is on the relative agreement of two features of the probability density $\phi(x, t)$. First, we compare the predicted steady state maximum and minimum values of the probability density on the spatial domain; Φ_c (at the cold region) and Φ_h (at the hot region) respectively. Second, we compare the predicted relaxation times for the system to approach a steady state probability density. Particular attention is given to the agreement between either method as the frictional dissipation coefficient γ is varied over several orders of magnitude.

In figure 2 we present the x dependence of the probability density $\phi(x, t)$ at several different moments of time as determined by the FVM solution of the Smoluchowski equation. The considered crystalline potential and surface temperature distribution are those given in Eq. (1) and (2) respectively. The simulation parameters are T_0 = 500 K, ΔT = 400 K, λ = 250 nm (500 nm laser), $V_0 = k_B T_0/0.15$, $\gamma = 10^{10}$ s^{-1}, m = 100 amu (atomic mass units) and a = 2 Å. The spatial domain is across one full period of the temperature modulation; $0 < x \leq 250$ nm. The curves represent the moments of time t = 200 ns (curve 1), 600 ns (curve 2), 1000 ns (curve 3), and 2000 ns (curve 4). The particles are randomly distributed at $t = 0$, such that $\phi(x, 0) = \phi_0$ = const. The lower temperature of 500 K is considered greater than room temperature to account for an increase in the average temperature of the surface that is predicted when heating a metallic film with interfering laser pulses [2]. These curves reveal the essential features that have been previously reported [1]. The probability density evolves such that there is a maximum at the position corresponding to the minimum temperature (at $x = \lambda/2$, where $T = T_0$), and a minimum at the position of maximum temperature (at $x = 0$ and λ, where $T = T_0 + \Delta T$). A steady state of the probability density occurs at large times (see curve corresponding to 2000 ns) which shows strong redistribution of particles to the colder regions on the substrate. In this figure, the ratio of the probability density in the cold regions to that in the hot regions approaches $\Phi_c / \Phi_h \sim 25$. Interestingly, this numerical method also reveals the fine structure of the probability density evident in the two maxima that merge together (see the curve corresponding to 200 ns) – this has been predicted by our previous Monte Carlo simulations [1] and is an important feature of the temporal evolution of $\phi(x, t)$. This fine structure has been shown to be most pronounced at strong potential of interaction between the particles and the surface i.e. when V_0 is large.

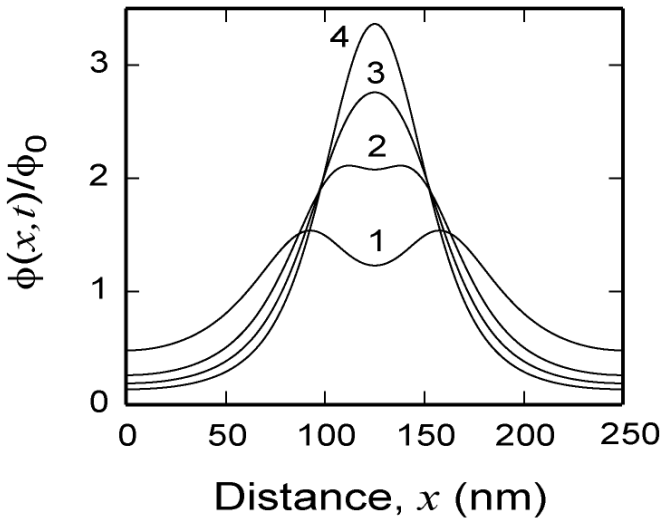

Figure 2: Evolution of the normalized probability density function □(*x*,*t*) for particle *x*-coordinates on the surface; ϕ_0 is the initial uniform probability density for the particles at *t* = 0. The four different curves correspond to the moments in time *t* = 200 ns (curve 1), 600 ns (curve 2), 1000 ns (curve 3), and 2000 ns (curve 4). The other parameters are T_0 = 500 K, ΔT = 400 K, λ = 250 nm, $V_0 = k_B T_0/0.15$, $\gamma = 10^{10}$ s^{-1}, *m* = 100 amu (atomic mass units), and *a* = 2 Å. Particles are seen to migrate toward the cold region centered at *x* = 125 nm, and are strongly redistributed on the surface.

It should be noted that the strength of redistribution of particles to the cold regions can be many orders of magnitude greater than that which would be observed for free particles (V_0 = 0). For example, under similar conditions but with V_0 = 0, we would expect only $\Phi_c / \Phi_h \sim 2$ [1]. The existence of potential wells acting as particle traps strongly reduces the flux of particles migrating back into the hot regions. Particles in the cold regions can be effectively immobile due to very low jump rates. At the same time, particles in the hot regions are easily thermally activated to escape potential wells and migrate to the cold regions. The result is a massive migration of particles into the cold regions as the system evolves toward the steady state

probability density. Thermal tweezers is therefore most effective for material systems with strong particle-surface interactions.

In figures 3 (a) and 3 (b) we present a comparison of the steady state values of the maximum and minimum of the probability density (Φ_c and Φ_h) as predicted by each method for the frictional dissipation coefficients varying from $\gamma = 10^9$ s^{-1} to $\gamma = 10^{12}$ s^{-1}. All other parameters are the same as in figure 2 except that $V_0 = k_B T_0/0.3$. The data points with error bars represent the predictions of the MC simulations; the solid curves represent the predictions of the Smoluchowski equation approach. In the MC simulations, the trajectories of 50,000 particles are calculated which is about the number required to determine smooth curves of $\phi(x, t)$. The presence of an error bar at each data point is associated with the stochastic nature of the MC approach. Particle trajectories are simulated for large enough time to determine asymptotic values of Φ_c and Φ_h to a desired accuracy by analysis of fitted curves. The size of error bars indicate the error in determining the asymptote of the curve *chosen to fit the data*. Inspection of the scale on the *y* axes of figure 3 reveals that these errors are quite small, typically ~ 5%. At the same time, curves fitted to plots of Φ_c or Φ_h versus time are typically exponential or sigmoidal; though each of these functions most likely cannot describe the true dynamics of Φ_c or Φ_h. The actual dependence of Φ_c and Φ_h is a complicated function of time which is evident from the fine structure of the probability density during non-steady state conditions as discussed above (see figure 2). Therefore intrinsic inaccuracy is associated with curve fitting the dependencies as just exponential or sigmoidal. We are unable to predict the significance of this error case by case and therefore this error is not included in the error bars.

Comparing the relative agreement between each method with regard to their predicted values of Φ_c and Φ_h, we first give attention to the range $\gamma > 10^{10}$ s^{-1} in figures 3 (a) and 3 (b). Considering the error bars, the MC simulation predictions of Φ_c in figure 3 (a) are

systematically less than the SE predictions by ~ 5%. In figure 3 (b), we see that the MC simulation predictions of Φ_h are systematically larger and within ~ 25% compared to predictions by the SE. Therefore over this range, the quantitative agreement between either method is reasonable. The systematic difference observed between the two methods may be the choice of curves used to fit the data points. We predict that asymptotic values of the true dependencies (see discussion above) would more closely reflect the curve predicted by from the SE.

Now consider the range $\gamma < 10^{10}\ s^{-1}$. It is obvious that in this range the MC predictions rapidly depart rapidly from those of the SE as γ decreases. The MC calculations predict the existence of an "optimal" value of γ where Φ_c is a maximum and Φ_h a minimum; that is, where the redistribution of particles is the strongest compared to frictions outside of this range. On the other hand, the SE does not predict an optimal value of γ at all. Rather, it predicts simply a monotonic increase of Φ_c and monotonic decrease of Φ_h as γ is decreased. To understand the dependence on γ relative to each of these methods we need to consider carefully the conditions at steady state.

Even at steady state conditions, there is an average flux of particles moving in both directions; hot → cold, and cold → hot. Though in steady state, the total flux into a spatial increment is equal to the total flux out of the spatial increment; therefore ϕ remains constant across all spatial increments and the probability density no longer evolves in time. Broadly speaking, we can say that the flux of particles from the hot regions toward the cold regions is equal and opposite to the flux from the cold regions to the hot regions. On the other hand, the diffusion rate of individual particles from hot to cold is typically much greater than the rate of diffusion from cold to hot – due to the relative jump rates and jump lengths in either region. For the fluxes to cancel, there must be an imbalance in the particle concentration; specifically $\Phi_c >> \Phi_h$. This is the origin of the steady state thermophoretic redistribution of particles.

Now consider as the friction is increased such that $\gamma > 10^{10}$ s^{-1}. It can be seen in figures 3 (a) and 3 (b) that both approaches predict that Φ_c decreases while Φ_h increases; that is, the particles become less strongly redistributed as γ increases. Primarily this indicates a reduction of the difference between the particle diffusion rate from hot → cold and the diffusion rate from cold → hot. As γ is increased there is a transition to where the particle motion is almost solely due to nearest neighbour hopping. In this regime, the diffusion rate is only a function of the *jump rate* (the rate at which particles escape from a well). The jump length is constant over the entire spatial domain and is equal to the lattice spacing *a*. The jump rate is related to the surface temperature approximately by an Arrhenius type relationship of the form $\exp(-2V_0/k_BT)$. It is also related to the friction γ by a more complicated dependence [7, 17] that reduces as γ^{-1} in the high friction ($\gamma >> \omega_0$) and low friction ($\gamma << \omega_0$) regimes – ω_0 is a parameter describing the typical oscillation frequency of particle motion in the potential wells. In the intermediary friction regime ($\gamma \sim \omega_0$) there is weaker dependence of the diffusion rate on the friction. In any case, the diffusion rate monotonically increases with decreasing friction. Since the strength of modulation of ϕ (*x*, *t*) (specifically the ratio Φ_c/Φ_h) is directly proportional to the difference in the hot → cold and cold → hot diffusion rates, we therefore expect Φ_c/Φ_h to decrease monotonically with increasing friction. Indeed, this is predicted over the entire range of friction we consider by the Smoluchowski equation.

Let us now consider more closely the range where $\gamma < 10^{10}$ s^{-1}. Here, there is a significant disagreement between each of the methods with increasing divergence as γ is decreased. As discussed, the SE predicts continuing increase in strength of particle redistribution; on the other hand, MC simulations predict a decrease in modulation of ϕ (*x*, *t*) at steady state. In this range of γ, long jumps must be considered in the diffusion rate of individual particles. The jump length increases with decreasing friction, to the regime where particle motion is effectively that of a Brownian particle in a viscous fluid. In the MC

simulations, long jumps are always considered; they are simply resolved in calculation of particle trajectories. On the other hand, our implementation of the FVM in the solution of the SE is only useful when the jump lengths are much less than wavelength of the laser. When the jump length is of the order of the wavelength of the laser ($l \sim \lambda$), the predictions of the Smoluchowski equation will not be accurate. Indeed, the existence of large Lévy flights invalidates the assumption of Fickian diffusion. Under these conditions a fractional diffusion model would be expected, however, this is well outside the scope of this paper [18]. Therefore, the divergence between predictions of either method is expected when $l \sim \lambda$, and in this regime ($\gamma < 10^{10}$ s^{-1} for the presented results) we rely on MC simulations for a more accurate picture of particle dynamics.

The existence of an optimal friction where the ratio Φ_c/Φ_h is a maximum, and subsequent decrease of Φ_c/Φ_h as the friction is decreased from the optimal value, are two interesting observations that should be discussed further. The maximum value of Φ_c/Φ_h indicates the relative difference between the hot → cold and cold → hot diffusion rates is larger than for frictions outside of the optimal range. We predict that over the optimal range of γ, the jump length makes a significant contribution to the diffusion rate in migration of particles from hot → cold – the long jumps will act to increase the diffusion rate. At the same time, particles escaping from the cold region remain in almost a nearest-neighbour hopping regime. The fact that the diffusion regime is different in the hot region compared to the cold region would result in a significant difference in the hot → cold and cold → hot diffusion rates with an associated increase in the ratio Φ_c/Φ_h. On the other hand, as the friction is further decreased below the optimal range, the jump length in the hot regions will become of the order of λ, the period in the temperature modulation. This may result in particles escaping from the hot region effectively jumping over and "missing" the cold region. A full investigation of this phenomenon is beyond the scope of this paper, and will be presented in a

future publication [10]. It should also be mentioned that as γ is decreased to well below the optimal range, there is a transition to the diffusion regime of a Brownian particle diffusing in a viscous fluid. In this case, the particle effectively does not see the crystalline potential of the substrate. This diffusion regime is practically equivalent to that of free particles, which are shown to be very poorly redistributed by thermal tweezers [1].

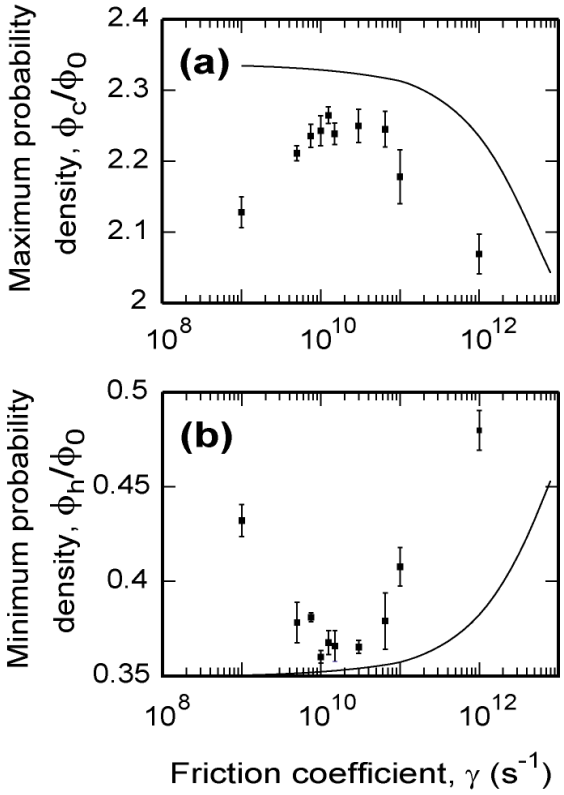

Figure 3: Dependence on the frictional dissipation coefficient γ of the steady state maximum Φ_c (a) and minimum Φ_h (b) of the non-normalized probability density and as predicted by Monte Carlo simulations (data points) and the finite volume solution of the Smoluchowski equation (solid curves). Reasonable agreement is seen to extend only to the friction range $\gamma > 10^{10}$ s^{-1}, with divergence between the predictions of either method as γ is decreased below 10^{10} s^{-1}. This has been explained due to long jumps of particles on the scale of the temperature modulation λ in the low friction range. It can also be seen that the MC simulations predict an optimal value of γ where

particle redistribution is the strongest. The parameters are the same as for figure 2 except that $V_0 = k_B T_0/0.3$.

In figures 4 (a) and 4 (b) we present the predicted relaxation times τ_c and τ_h of Φ_c and Φ_h for the same range $10^9\,s^{-1} \le \gamma \le 10^{12}\,s^{-1}$. All other parameters are the same as for figure 3. Once again, the data points indicate the predictions of the MC simulations, and the solid curves are the prediction of the FVM solution of the Smoluchowski equation. Error bars are mostly omitted since typically the error is less than the size of the data point itself. In both figures we see that the SE predicts monotonic, exponential type increase of the relaxation time with increasing γ. This predicted increase in τ_c and τ_h is trivial, simply being related to a lower diffusion rate of particles toward the cold region. On the other hand, the MC simulations show an unusual dependence where both τ_c and τ_h monotonically increase with increasing friction when $\gamma > 10^{10}\ s^{-1}$, and with decreasing friction when $\gamma < 10^{10}\ s^{-1}$; that is, there is a minimum in the relaxation time which actually corresponds to a maximum in the strength of particle redistribution Φ_c/Φ_h. The increase in the relaxation times τ_c and τ_h at low friction support the previously discussed idea that long jumps $l \sim \lambda$ mean the particle effectively misses the cold region. Additionally, at low friction it is well known that the probability of thermal activation of particles to escape from potential wells is reduced. In this case, particles with very low jump rates will need to make many jumps to become effectively trapped in the cold region; in this scenario the relaxation time of $\phi(x, t)$ will be dramatically increased (see [10] for further discussion).

Let us now compare quantitatively the agreement between each approach with regard to the relaxation times τ_c and τ_h. Firstly drawing attention to τ_c in figure 4 (a), we see that agreement between the two methods diverges with increasing friction. At $\gamma = 10^{12}\,s^{-1}$, the MC simulation approach predicts ~ 50% smaller relaxation time than the SE. We believe this

disagreement is related to the complicated dependence of Φ_c on time, due to the fine structure in the evolution of $\phi(x, t)$ previously discussed. Particularly, the choice of simple sigmoid or exponential function to asymptotically determine the relaxation time is not sufficient. Additionally, at large frictions of $\gamma > 10^{11}$ s^{-1} the MC calculations verge on impractical when considering the large number of particles that must be simulated to determine accurately the probability density $\phi(x, t)$. In this case, it can be difficult to obtain sufficient data points to determine accurately the dependence of Φ_c or Φ_h on time, which further increases errors related to curve fitting. In the lower friction range, $\gamma \leq 10^{10} s^{-1}$, there is a departure in the predicted trends of the relaxation times due to the presence of long jumps in the particle diffusion, which are not properly resolved in the FVM solution of the SE – see previous discussion.

Now drawing attention to the dependence of the relaxation time of Φ_h on γ in figure 4 (b), it is observed that the relative agreement between either method is excellent except in the previously discussed low friction range, $\gamma \leq 10^{10} s^{-1}$. It is interesting to consider why this is the case compared to the relative disagreement observed in figure 3 (a). The absolute values of the relaxation times should be compared; it can be seen that τ_c is typically greater than τ_h including by up to ~ 100%. A simple explanation is related to a less complicated dependence of Φ_h on time. Indeed, in the evolution of the probability density particles migrate rapidly away from the hot region. On the other hand, we can consider that particles from all regions diffuse to the position of minimum temperature $x = \lambda/2$. Since the diffusion rate is varied along the path from the hot regions to the cold regions, there is an interesting scenario within each spatial increment. Consider for example the average particle migration in the positive x direction from anywhere in the range $0 \leq x < \lambda/2$ toward $x = \lambda/2$. If we divide this region into discrete spatial increments, we expect that during the evolution of $\phi(x, t)$ there will an increased particle flux entering the west face of the increment compared to the flux of

particles leaving the increment through the east face. The result will be “waves” in the probability density that propagate toward the position of minimum temperature, similar to that observed in figure 1. Obviously this will result in a more complicated dependence of Φ_c on time compared to Φ_h. Therefore, asymptotic analysis of fitted exponential or sigmoidal curves will more accurately determine the relaxation time τ_h and there will be increased agreement with the predictions of the SE.

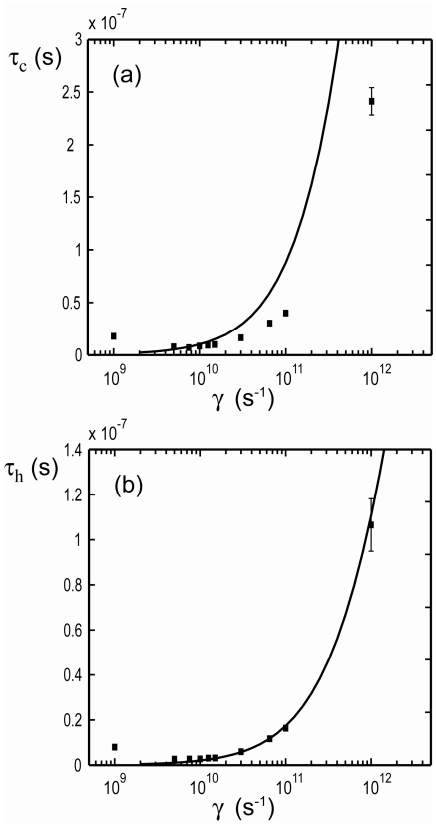

Figure 4: Dependence on the frictional dissipation coefficient γ of the relaxation times of the maximum τ_c (a) and minimum τ_h (b) of the probability density $\phi(x, t)$ as predicted by the Monte Carlo simulations (data points) and the finite volume solution of the Smoluchowski equation (solid curves). Similarly to in figure 3, reasonable agreement is seen to extend only to the friction range $\gamma > 10^{10}$ s^{-1}, with divergence between the predictions of either method as γ is decreased below 10^{10} s^{-1}. Specifically, the MC simulations predict a shortest relaxation

time corresponding to the optimal range of friction as demonstrated in figure 3. All parameters are the same as for figure 3.

Regarding computational efficiency, the FVM solution of the SE is typically many orders of magnitude faster than the MC simulations at determining the probability density $\phi(x, t)$. The MC approach is an inefficient approach to the problem due to the large spatial domain of the computational window required to span a full period of the temperature modulation, and the large timescale of the thermopheretic redistribution of particles. For example, to determine a smooth probability density from individual particle co-ordinates over a spatial domain of about ~ 100 × 100 nm^2, the simulation of ~ 50,000 particles is required. In addition, the discrete time step in the Ermak algorithm is dt ~ 10 fs, and typically the time scale of the simulation is ~ 100 ns to predict with reasonable accuracy the relaxation times τ_c, τ_h and the steady state maximum and minimum of the probability density (Φ_c and Φ_h) from asymptotic analysis of fitted curves. Therefore, unless details of the diffusive motion of individual particles are required, the preferred choice at first appears to be FVM solution of the SE. On the other hand, we have shown that the FVM solution SE is only appropriate for sufficiently high friction. Indeed, when the frictional dissipation parameter is in the range $\gamma \leq 10^{10}\,s^{-1}$ (more generally when $l \sim \lambda$) we have shown that the predictions of the two methods diverge with decreasing γ. This has been explained due to the inability for long jumps on the order of the temperature modulation to be properly resolved in the FVM. On the other hand, long jumps of this length scale are intrinsically considered in the solution of the LE and therefore this is the appropriate choice of method in this range. We stress that in the higher friction regime $\gamma > 10^{10}\ s^{-1}$ that the MC simulations are highly inefficient and the computation times border on impractical. As friction is increased, the relaxation times increase exponentially (see figure 4) which require the timescale of the MC simulations to be

dramatically increased to achieve steady state conditions. On the other hand, the FVM actually increases in efficiency as γ increases, and is believed to predict more accurately the probability density $\phi(x, t)$ due to complications with curve fitting in the statistical analysis of data obtained by the MC simulations.

4. Conclusions

We have presented two different numerical approaches for the theoretical investigation of thermal tweezers of adsorbed particles diffusing on substrates modelled as an uncoupled, square lattice, periodic potential with linear frictional dissipation. The temperature on the surface was considered to be strongly modulated sinusoidally along one direction. The two approaches were the Monte Carlo simulations of a Langevin equation, and a finite volume method solution of a Smoluchowski equation. In the MC simulations, the trajectories of many particles were calculated to accurately determine the temporal evolution of the probability density at arbitrary moments of time by statistical analysis of particle co-ordinates. In the second approach, a local effective mobility and diffusion constant was determined by the matrix continued fraction method algorithm applied to solve the Klein-Kramer equation. The diffusion constant was subsequently substituted into a Smoluchowski equation which was solved by the finite volume method.

We conclude that the FVM is typically the primary choice of method due to its high computational efficiency compared to the Monte Carlo simulations, though its implementation here is only applicable at sufficiently high friction. As friction is decreased to $\gamma < 10^{10}$ s^{-1} (depending on various conditions), the predictions of both methods were shown to diverge. In this regime, the numerical solution of the Langevin equation is the appropriate

choice because it resolves long jumps of the particles on the scale of the period of the temperature modulation.

We also discussed two main predictions obtained by numerical solution of the Langevin equation which have so far not been reported. First, the existence of an optimal friction at which the strongest steady state redistribution of particles is obtained. Second, an unusual dependence of the relaxation time displaying a minimum value corresponding to the optimal friction. Physical explanation of these effects were briefly discussed, but a complete investigation will be presented in a future publication currently in preparation [10].

References

[1] D. K. Gramotnev, D. R. Mason, G. Gramotnev, et al., Applied Physics Letters **90**, 054108 (2007).

[2] D. R. Mason, D. K. Gramotnev, and G. Gramotnev, Journal of Applied Physics **104**, 064320 (2008).

[3] D. Braun and A. Libchaber, Physical Review Letters **89**, 188103 (2002).

[4] V. Garcés-Chávez, R. Quidant, P. J. Reece, et al., Physical Review B **73**, 085417 (2006).

[5] M. P. Allen and D. J. Tildesley, *Brownian Dynamics* (Oxford University Press, 1989).

[6] J. M. Sancho, A. M. Lacasta, K. Lindenberg, et al., Physical Review Letters **92**, 250601 (2004).

[7] T. Ala-Nissila, R. Ferrando, and S. C. Ying, Advances in Physics **51**, 949 (2002).

[8] W. D. Luedtke and U. Landman, Physical Review Letters **82**, 3835 (1999).

[9] O. M. Braun and R. Ferrando, Physical Review E **65**, 061107 (2002).

[10] D. R. Mason, D. K. Gramotnev, and G. Gramotnev.

[11] J. A. Thackham, D. L. S. McElwain, and I. W. Turner, Bulletin of Mathematical Biology **71**, 211 (2009).

[12] R. Zwanzig, *Brownian motion and Langevin equations, in nonequilibrium statistical mechanics* (Oxford University Press, 2001).

[13] H. Riskin, *The Fokker-Planck equation: methods of solution and applications* (Springer, 1989).

[14] R. Ferrando, R. Spadacini, and G. E. Tommei, Physical Review E **48**, 2437 (1993).

[15] R. Ferrando, M. Mazroui, R. Spadacini, et al., New Journal of Physics **19**, 1 (2005).

[16] G. Caratti, R. Ferrando, R. Spadacini, et al., Chemical Physics **235**, 157 (1998).

[17] L. Y. Chen and S. C. Ying, Physical Review B **49**, 13838 (1994).

[18] R. Metzler, A. V. Chechkin, and J. Klafter, in *arXiv*, (2007), Vol. arXiv:0706.3553v1.